Inorg. Chem. **2006**, *45*, 7555–7565

Forum

Template-Grown Metal Nanowires

Timothy R. Kline, Mingliang Tian,* Jinguo Wang,* Ayusman Sen,* Moses W. H. Chan,* and Thomas E. Mallouk*

Departments of Chemistry and Physics, Materials Research Institute, and Center for Nanoscale Science, The Pennsylvania State University, University Park, Pennsylvania 16802

Received January 23, 2006

The growth of metal nanowires using membranes as hard templates is reviewed. The method provides access to arrays of single-crystal metal nanowires and to quasi-one-dimensional metal nanostructures with controlled compositional variation along their length. Recent applications of these kinds of nanowires to problems in superconductivity, optical spectroscopy and sensing, and catalytic conversion of chemical to mechanical energy are reviewed.

Introduction

High-aspect-ratio metal nanostructures—nanorods, nanowires, and nanotubes—are the subject of much current study. Although metals are "old" materials, their fabrication in new forms, particularly at the nanoscale, opens up new ways to study their physical and electronic properties. There are potential applications in which a metal or metal-containing composite nanowire can replace a more conventional device, for example, in microelectronic circuits or magnetic memories. More interestingly, as quasi-one-dimensional (1-D) nanostructures, metal nanowires and nanotubes reveal new physical and chemical phenomena that are a direct consequence of their size, shape, and reduced dimensionality. These novel properties promise ultimately to be of even greater technological impact because they will enable genuinely new kinds of devices and applications.

This paper reviews recent advances in the synthesis of metal nanowires in hard templates and the unusual properties that emerge as a consequence of their confinement to nanoscale dimensions. We focus primarily on our recent efforts to examine some of the unique phenomena, in particular, novel superconducting and optical properties, the dynamics of nanowire assembly, and catalyzed motion, that have been observed with metallic nanowires.

* To whom correspondence should be addressed. E-mail: mut1@psu.edu (M.T.), asen@psu.edu (A.S.), chan@phys.psu.edu (M.W.H.C.), tom@chem.psu.edu (T.E.M.).

Growth of Metal Nanowires in Hard Templates

The synthesis of 1-D nanostructures has been recently reviewed by Xia et al.[1] While an impressive variety of techniques now exist for making metal nanostructures, the two most general are the so-called soft- and hard-template methods. In the soft-template method, metal nanowire growth occurs by chemical or electrochemical reduction, usually in a solution that contains surfactants or other structure-directing molecules. Depending on the nature of the soft template, its effect is to inhibit the growth of certain crystal faces of the metallic crystal or to alter the transport of reagents to certain faces. Different variations of the soft-template method are direct electrochemical reduction,[2] seeding followed by chemical reduction,[3] and redox reactions that transform a starting material that is easily grown as a nanowire (such as Se or Ag) into a different metal or compound.[4] When combined with selective etching of the core material, this method can be used to make cylindrical nanotubes as well as open prismatic nanostructures with interesting plasmonic

(1) Xia, X.; Yang, P.; Sun, Y.; Wu, Y.; Mayers, B.; Gates, E.; Yin, Y.; Kim, F.; Yan, H. *Adv. Mater.* **2003**, *15*, 353.
(2) Yu, Y.; Chang, S.; Lee, C.; Wang, C. R. C. *J. Phys. Chem. B* **1997**, *101*, 6661.
(3) (a) Murphy, C. J.; Jana, N. R. *Adv. Mater.* **2002**, *14*, 80. (b) Jana, N. R.; Gearheart, L.; Murphy, C. J. *J. Phys. Chem. B* **2001**, *105*, 4065.
(4) (a) Gates, B.; Wu, Y.; Yin, Y.; Yang, P.; Xia, Y. *J. Am. Chem. Soc.* **2001**, *123*, 11500. (b) Gates, B.; Mayers, B.; Wu, Y.; Sun, Y.; Cattle, B.; Yang, P.; Xia, Y. *Adv. Funct. Mater.* **2002**, *12*, 679. (c) Sun, Y.; Mayers, B.; Xia, Y. *Nano Lett.* **2002**, *2*, 481.

10.1021/ic0601384 CCC: $33.50
Published on Web 09/11/2006

behavior.[5] An important advantage of the soft-template method is that it is scalable to bulk quantities of nanowires, especially when the reduction is done chemically in solution.

In the hard-template method, an inorganic material or polymer, typically in the form of a porous membrane, acts as rigid mold for the chemically or electrochemically grown replica. Because the template is usually a thin membrane, this method is difficult to scale-up to macroscopic quantities of nanowires, although efforts in that direction are underway.[6] The benefit of the hard-template method, which is the focus of our research and the subject of this review, is its ability to produce complex 1-D nanostructures. The hard template allows for unidirectional growth, making it easy to vary the composition of the nanowire or nanotube in the axial direction. With vertical pores, one obtains aligned arrays of nanowires, which simplify bulk transport measurements and enable certain special applications, such as chemical sensor, field emitter,[7] and magnetic nanowire arrays. Nanowires made by replication of horizontal pores (such as cracks[8] or steps[9] in planar substrates) are easily top-contacted for electrical measurements and can, in principle, be patterned in complex ways to make sensor arrays or nanoscale circuits.

The growth of metal nanowire arrays in hard templates was first reported by Possin, who electroplated nanowires of Sn, In, and Zn into nanopores made by etching of nuclear particle damage tracks in sheets of natural mica crystals.[10] Giordano and co-workers, who studied electron localization in Pt and Ag nanowires, later refined this technique to obtain nanowires with diameters below 10 nm.[11] Subsequent research has made extensive use of track-etched polycarbonate[12] and anodic aluminum oxide (AAO) templates,[13,14] which are produced and sold commercially as filters. In the case of the track-etched polymer membranes, the pore diameter is controlled by the etching time and conditions, whereas the applied voltage is the most important factor in determining the size and spacing of pores in AAO. An important advance in the AAO method was the discovery of techniques for making hexagonally ordered pore arrays,[15] which enabled subsequent research on structurally well-defined arrays of magnetic nanowires, field emitters, and single-electron tunneling devices. The original method for making regular pore arrays in AAO involved growing and then stripping off a sacrificial oxide layer; the resulting pattern in the underlying Al is transferred to the porous oxide film in the next anodization cycle. Very highly ordered arrays of pores in AAO have recently been made by first indenting the Al in the desired pattern and then anodically etching at the appropriate voltage.[16]

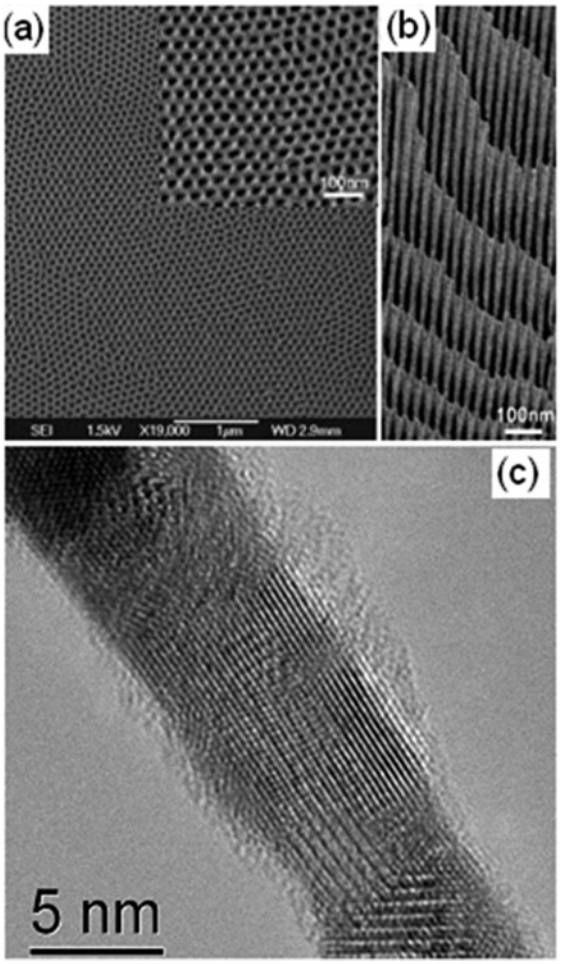

Figure 1. (a) Field emission scanning electron microscopy image of the bottom surface, after ion milling, of a free-standing AAO film anodized at 22 V and 0−3 °C from an Al foil and detached by the reverse-bias method. (b) Cross-sectional image of the AAO film. (c) HRTEM image of a 7.2-nm Au wire grown small-pore AAO and released by dissolution of the membrane.

Figure 1 shows images of nanopore arrays in AAO. When Al is anodized in acidic solutions, an insulating oxide layer separates the bottom of the vertical pore from the underlying metal electrode. With this barrier layer present, alternating current methods must be used to electrodeposit metals into the pores. If the pores are opened at the bottom, direct current (dc) deposition and interrogation of the nanowire array,

(5) Sun, Y.; Mayers, B.; Xia, Y. *Adv. Mater.* **2003**, *15*, 641.
(6) Gerein, N. J.; Haber, J. A. *J. Phys. Chem. B* **2005**, *109*, 17372.
(7) Davydov, D. N.; Sattari, P. A.; Al-Mawlawi, D.; Osika, A.; Haslett, T. L.; Moskovits, M. *J. Appl. Phys.* **1999**, *86*, 3983.
(8) Adelung, R.; Aktas, O. C.; Fran, J.; Biswas, A.; Kunz, R.; Elbahri, M.; Kanzow, J.; Schürmann, U.; Faulpel, F. *Nat. Mater.* **2004**, *3*, 375.
(9) (a) Zach, M. P.; Ng, K. H.; Penner, R. M. *Science* **2000**, *290*, 2120. (b) Walter, C. J.; Murray, B. J.; Favier, F.; Kaltenpoth, G.; Grunze, M.; Penner, R. M. *J. Phys. Chem. B* **2002**, *106*, 11407. (c) Penner, R. M. *J. Phys. Chem. B* **2002**, *106*, 3339.
(10) (a) Possin, G. E. *Physica* **1971**, *55*, 339. (b) Possin, G. E. *Rev. Sci. Instrum.* **1970**, *41*, 772.
(11) (a) Williams, W. D.; Giordano, N. *Rev. Sci. Instrum.* **1984**, *55*, 410. (b) Madsen, J. T.; Giordano, N. *Phys. Rev. B* **1985**, *31*, 6395.
(12) Penner, R. M.; Martin, C. R. *J. Electrochem. Soc.* **1986**, *133*, 2206.
(13) Al-Mawlawi, D.; Liu, C. Z.; Moskovits, M. *J. Mater. Res.* **1994**, *9*, 1014.
(14) (a) Martin, C. R. *Chem. Mater.* **1996**, *8*, 1739. (b) Martin, C. R. *Science* **1994**, *266*, 1994.
(15) (a) Masuda, H.; Fukuda, K. *Science* **1995**, *268*, 1466. (b) Zhang, L.; Cho, H. S.; Li, F.; Metzger, R. M.; Doyle, W. D. *J. Mater. Sci. Lett.* **1998**, *17*, 29. (c) Jessensky, Q.; Muller, F.; Gosele, U. *Appl. Phys. Lett.* **1998**, *72*, 117. (d) Li, F.; Zhang, L.; Metzger, R. M. *Chem. Mater.* **1998**, *10*, 247.
(16) (a) Masuda, H.; Yamada, H.; Satoh, M.; Asoh, H.; Nakao, M.; Tamamura, T. *Appl. Phys. Lett.* **1997**, *71*, 2770. (b) Masuda, H.; Asoh, H.; Watanabe, M.; Nishio, K.; Nakao, M.; Tamamura, T. *Adv. Mater.* **2001**, *13*, 189. (c) Choi, J.; Nielsch, K.; Reiche, M.; Wehrspohn, R. B.; Gösele, U. *J. Vac. Sci. Technol. B* **2003**, *21*, 763. (d) Fournier-Bidoz, S.; Kitaev, V.; Routkevitch, D.; Manners, I.; Ozin, G. A. *Adv. Mater.* **2004**, *16*, 2193. (e) Sander, M. S.; Coté, M. J.; Gu, W.; Kile, B. M.; Tripp, C. P. *Adv. Mater.* **2004**, *16*, 2052.

which is more convenient for many applications, is possible. To perforate the oxide barrier layer, the voltage is decreased progressively at the end of the anodic etching procedure. However, this isotropic etching inevitably results in widening of the pores, making it difficult to fabricate membranes with pore diameters of less than 10 nm.

Because much of the interesting physics of metal, semiconducting, and superconducting nanowires emerges at very fine diameters, there is a need for membranes with narrower pores. Recently, it has been shown that the AAO barrier layer can be removed selectively, without widening the pores, by applying a cathodic potential at the end of the electrodeposition.[17,18] Figure 1 shows an image of a 7-nm-diameter Au wire grown in such a template and then released by etching the membrane. This method now enables one to make <10-nm-diameter nanowires of many different metals in parallel arrays, at a density of about 10^{11} wires/cm^2. To access even smaller dimensions and higher densities, a "pore within a pore" method has been developed. Here, a mesoporous silicate, SBA-15, is grown inside the larger pores of AAO. Confinement in AAO serves to align the normally randomly oriented pores of the mesoporous silicate perpendicular to the plane of the membrane. These pores can be filled with metals to obtain parallel nanowires or other interesting shapes, such as helical nanowires, with diameters as small as 6−7 nm.[19−21]

Control of the purity, crystallinity, and texture is important for electronic studies of metals and superconductors because impurity and grain boundary scattering can dominate electronic transport, particularly at very low temperatures. Although electroplated metal films are normally polycrystalline, the same plating solutions and procedures can afford arrays of single crystals in hard templates. This is because, at a given current density, the nucleation rate is proportional to the cross-sectional area of the nanowire, but the vertical growth rate is independent of the area. Soft metals such as Au,[22] Sn,[23] Zn,[24] Ag,[25] Pb,[26] Bi,[27] and Cu[22,25] can be grown as arrays of single crystals when the pore diameter is less than about 70 nm. High-resolution TEM (HRTEM) images of Au nanowires show that they are faceted at the tip, exposing low-index faces to minimize the surface energy.[25] A polymeric surfactant (gelatin) and a slightly elevated growth temperature (40 °C) promote surface diffusion of atoms and favor the growth of existing crystal nuclei. Single crystals, or twinned nanowires with long single crystalline sections, are obtained by electroplating at low overpotential to minimize the nucleation rate.[22] In contrast, metals with higher melting points (Co, Ni, and Rh) invariably grow as polycrystalline nanowires even in very small pores. The higher metal−metal bond energies of these metals result in a smaller critical dimension for 2D nucleation and inhibit the diffusion of electrodeposited atoms on the surface.

With noble metals such as Au, Ag, Pd, and Pt, the growth of nanowires is not complicated by the formation of oxide layers in or around the wire. However, with more active metals such as Zn, Sn, Bi, Pb, and Cu, the formation of oxides is difficult to avoid, especially when the wires are released by etching away the membrane. Zn nanowires, which have interesting superconducting properties (see below) must be grown at low overpotential and at low temperature (19 °C) in order to obtain single crystals. An epitaxial ZnO layer, which probably forms when the nanowires are released from the template for imaging by TEM, is found around the Zn core. At higher overpotential, nucleation is fast and polycrystalline Zn wires are obtained, again with a ZnO outer layer. Increasing the deposition temperature gives wires that contain ZnO segments, as well as pure ZnO nanowires. In this case, oxidation of the Zn by protons in the electrolyte competes with reduction of Zn^{2+} ions to Zn.[24]

When multicomponent nanowires are grown by first plating one metal and then another, the microstructure and interdiffusion of the resulting junctions can become quite complex. Figure 2 shows an electron micrograph of a nanowire plated in the sequence Au−Sn−Au, with locally enlarged images of the junctions.[28] In the top junction, the Au segment is thinner near the junction, where progressively Sn-rich alloys (AuSn followed by $AuSn_4$) form along the wire. The thinning of the Au reflects the fact that its diffusivity is higher than that of Sn. A short oxide segment appears between the $AuSn_4$ and Sn segments. In the bottom junction, no intermetallic phases are detected, possibly because the SnO_2 region blocks diffusion of Au. "Striped" nanowires such as that shown in Figure 2 can be grown by plating from a solution that contains one metal and then replacing the solution to plate another metal.[29] An alternative procedure is to modulate the potential in a solution that contains two different metal ions.[30] The less active metal is deposited at low overpotential, and both metals are deposited at high overpotential. Typically, the more active metal is used in excess so that the segments grown at high overpotential contain predominantly that metal. One metal can be selec-

(17) Rabin, O.; Herz, P. R.; Lin, Y. M.; Akinwane, A. I.; Croniun, S. B.; Dresselhaus, M. S. *Adv. Funct. Mater.* **2003**, *13*, 631.
(18) Tian, M.; Yu, S.; Wang, J.; Kumar, N.; Wertz, E.; Li, Q.; Campbell, P.; Chan, M. W. H.; Mallouk, T. E. *Nano Lett.* **2005**, *5*, 697.
(19) Lu, Q.; Feng, G.; Komarneni, S.; Mallouk, T. E. *J. Am. Chem. Soc*. **2004**, *126*, 8650.
(20) Wu, Y.; Cheng, G.; Katsov, K.; Sides, S. W.; Wang, J.; Tiang, J.; Fredrickson, G. H.; Moskovits, M.; Stucky, G. D. *Nat. Mater.* **2004**, *3*, 816.
(21) Wu, Y.; Livneh, T.; Zhang, Y. X.; Cheng, G.; Wang, J.; Tang, J.; Moskovits, M.; Stucky, G. D. *Nano Lett.* **2004**, *4*, 2337.
(22) Wang, J.; Tian, M.; Mallouk, T. E.; Chan, M. W. H. *J. Phys. Chem. B* **2004**, *108*, 841.
(23) Tian, M.; Wang, J.; Snyder, J.; Kurtz, J.; Liu, Y.; Schiffer, P.; Mallouk, T. E.; Chan, M. W. H. *Appl. Phys. Lett.* **2003**, *83*, 1620.
(24) Wang, J.-G.; Tian, M.-L.; Kumar, N.; Mallouk, T. E. *Nano Lett.* **2005**, *5*, 1247.
(25) Tian, M.; Wang, J.; Kurtz, J.; Mallouk, T. E.; Chan, M. W. H. *Nano Lett.* **2003**, *3*, 919.
(26) Dubois, S.; Michel, A.; Eymery, J. P.; Duvail, J. L.; Piraux, L. *J. Mater. Res.* **1999**, *14*, 665. Michotte, S.; Piraux, L.; Dubois, S.; Pailloux, F.; Stenuit, G.; Govaerts, J. *Physica C* **2002**, *377*, 267.
(27) Yang, F. Y.; Liu, K.; Hong, K. M.; Reich, D. H.; Searson, P. C.; Chien, C. L. *Science* **1999**, *284*, 1335. Heremans, J.; Thrush, C. M.; Lin, Y. M.; Cronin, S.; Zhang, Z.; Dresselhaus, M. S.; Mansfield, J. F. *Phys. Rev. B* **2000**, *61*, 2921. Zhang, Z. B.; Sun, X. Z.; Dresselhaus, M. S.; Ying, J. Y.; Heremans, J. *Phys. Rev. B* **2000**, *61*, 4850.
(28) Wang, J.-G.; Tian, M.-L.; Mallouk, T. E.; Chan, M. W. H. *Nano Lett.* **2004**, *4*, 1313.
(29) Martin, B. R.; Dermody, D. J.; Reiss, B. D.; Fang, M.; Lyon, L. A.; Natan, M. J.; Mallouk, T. E. *Adv. Mater.* **1999**, *11*, 1021.

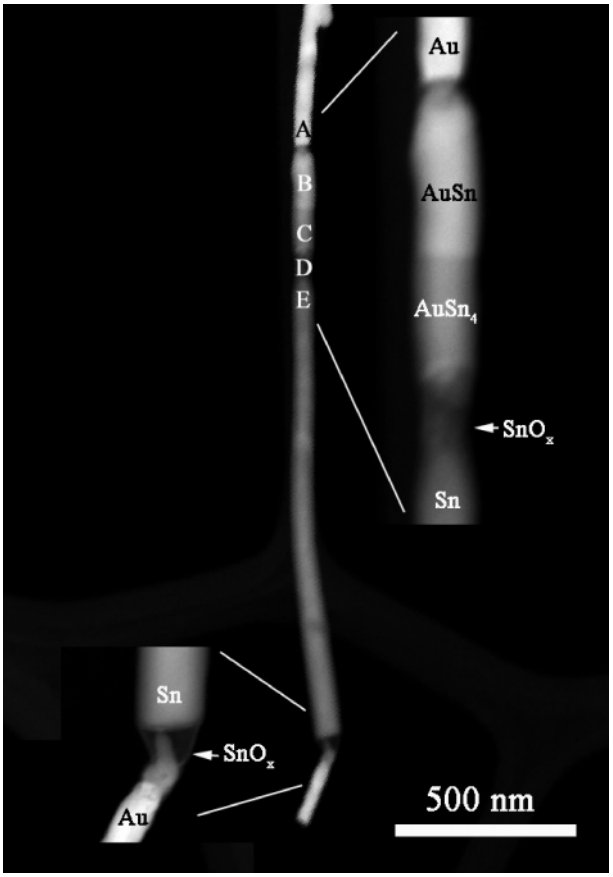

Figure 2. Scanning TEM annular dark-field image of a multisegment nanowire grown in the sequence Au−Sn−Au, after release from the template polycarbonate membrane. Locally enlarged images of the top Au−Sn and bottom Sn−Au junctions are shown as insets.

tively etched to give porous or notched nanowires.[31] Alternatively, metals can be plated into pores that contain colloidal spheres, which can later be dissolved to leave nanowires with spherical voids.[32]

Electronic Properties of Metal Nanowires

The hard-template method has been used to grow metal nanowires with semiconductor and conducting polymer segments by sequential electrodeposition. When in-wire self-assembly (e.g., of thiolated molecules on the tips of Au nanowires) is combined with sequential metal deposition steps, free-standing wires that contain junctions only one molecule thick have been made and studied. Layer-by-layer assembly of polymers, clusters, semiconductor nanoparticles, and other electronically active components has been combined with electrochemical wire growth in hard templates to make a wide variety of in-wire junctions and concentric shell structures. The electronic properties of nanowire diodes, transistors, and molecular junctions made by the hard-template method have been recently reviewed.[33,34] In these devices, the metal acts as an ohmic or rectifying contact and provides a way to make macroscopic contacts to a nanoscale electronic device. Electronic transport within the metal nanowire itself is not a phenomenon of particular interest in these studies.

At low temperatures, however, the electronic properties of quasi-1-D metallic structures are of substantial interest and have been studied for decades. Although all metals become superconducting at sufficiently low temperature, in a strictly 1-D system the transition to a superconducting phase should not occur. The crossover from bulklike to quasi-1-D behavior depends on the temperature-dependent phase coherence length $\zeta(T)$, which is the distance over which electrons are paired in the superconducting state. The value of $\zeta(0)$ is different for different superconductors. Despite extensive studies of superconductivity in dimensionally confined materials, there is still some controversy about what to expect in 1-D systems.[35−40] A major reason this problem has been difficult to sort out experimentally is the role of defects and grain boundaries in polycrystalline, amorphous, and granular samples. The availability of arrays of single crystals, which are protected from oxidation by the hard template, provides experimental access to questions about the effects of 1-D confinement.

We have studied single-crystal nanowires of Sn and Zn, which have $\zeta(0)$ values ($\sim$200 and 1−2 μm, respectively, in high-quality clean samples) that are 1−2 orders of magnitude larger than the diameters of the smallest nanowires available by the hard-template method. In these experiments, bulk Sn leads were used to contact wires that remained in the AAO or polycarbonate template. When sufficient pressure was applied to the Sn leads, good contact to the ends of the nanowires was achieved despite the possible presence of an oxide layer. This was evidenced by the fact that the resistance dropped to negligible values below T_c (3.7 K) with 100-nm-diameter wires. With this method, the transport properties of small collections of nanowires and even those of individual wires could be examined in two-point measurements. The experimental setup is shown schematically in Figure 3.[41]

A current-carrying state in a 1-D system is predicted to be metastable, and dissipation occurs when the system passes, through thermal activation or quantum tunneling, to a state of lower free energy separated by $2/\pi$ in phase. This process

(30) (a) Dubois, S.; Marchal, C.; Beuken, J. M.; Piraux, L.; Duvail, J. L.; Fert, A.; George, J. M.; Maurice, J. L. *Appl. Phys. Lett.* **1997**, *70*, 396. (b) Chen, M.; Searson, P. C.; Chien, C. L. *J. Appl. Phys.* **2003**, *93*, 8253. (c) Liu, K.; Nagodawithana, K.; Searson, P. C.; Chien, C. L. *Phys. Rev. B* **1995**, *51*, 7381. (d) Evans, P. R.; Yi, G.; Schwarzacher, W. *Appl. Phys. Lett.* **2000**, *76*, 481. (e) Choi, J.-r.; Oh, S. J.; Ju, H.; Cheon, J. *Nano Lett.* **2005**, 5, 2197.
(31) (a) Ji, C.; Searson, P. C. *Appl. Phys. Lett.* **2002**, *81*, 4437. (b) Qin, L.; Park, S.; Huang, L.; Mirkin, C. A. *Science* **2005**, *309*, 113. (c) Sioss, J. A.; Keating, C. D. *Nano Lett.* **2005**, *5*, 1779.
(32) Li, F.; He, J.; Zhou, W. L.; Wiley, J. B. *J. Am. Chem. Soc.* **2003**, *125*, 16166.
(33) Kovtyukhova, N. I.; Mallouk, T. E. *Chem.—Eur. J.* **2002**, *8*, 4354.
(34) Kushmerick, J. G.; Allara, D. L.; Mallouk, T. E.; Mayer, T. S. *MRS Bull.* **2004**, *29*, 396.
(35) (a) Giordano, N. *Phys. Rev. Lett.* **1988**, *61*, 2137. (b) Giordano, N. *Phys. Rev. B* **1990**, *41*, 6350.
(36) Rogachev, A.; Bezryadin, A. *Appl. Phys. Lett.* **2003**, *83*, 512.
(37) Giordano, N. *Phys. Rev. B* **1991**, *43*, 160.
(38) Sharifi, F.; Herzog, A. V.; Dynes, R. C. *Phys. Rev. Lett.* **1993**, *71*, 428.
(39) Lau, C. N.; Markovic, N.; Bockrath, M.; Bezryadin, A.; Tinkham, M. *Phys. Rev. Lett.* **2001**, *87*, 217003.
(40) Bezryadin, A.; Lau, C. N.; Tinkham, M. *Nature* **2000**, *404*, 971.
(41) Tian, M.; Wang, J.; Kurtz, J. S.; Liu, Y.; Chan, M. W. H.; Mayer, T. E.; Mallouk, T. E. *Phys. Rev. B* **2005**, *71*, 104521.

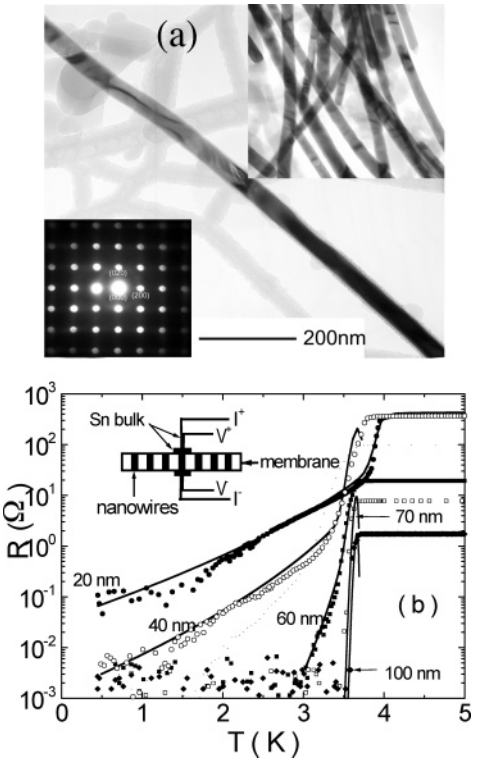

Figure 3. (a) TEM image of an individual 40-nm Sn nanowire. The insets are respectively the electron diffraction pattern of the wire showing [100] orientation and the TEM image of randomly distributed free-standing Sn wires. (b) Resistance vs temperature of 20-, 40-, 60-, 70-, and 100-nm nanowire arrays measured at the low current limit ($I < 1$ μA). The solid lines are theoretical fits based on the sum of the TAPS and QPS contributions to the resistance.

is called phase slip.[42,43] In the case of Sn wires, the superconducting transition temperature (T_c) at zero field is affected very little by confinement. Sn nanowires larger than 70-nm diameter show bulklike behavior in their $R-T$ curves (Figure 3), namely, a sharp drop in resistance at T_c and essentially zero resistance between T_c (3.7 K) and the limit of the measurement system (0.47 K). With 20- and 40-nm-diameter Sn wires, however, a residual resistance that persists down to at least 0.47 K signals the onset of quasi-1-D behavior.[41] Plots of log R vs T below T_c show two ohmic regions, which can be fit to models for thermally activated phase slip (TAPS) and quantum phase slip (QPS) near and below T_c, respectively. For 20- and 40-nm-diameter Sn wires, there is also evidence of quantum fluctuation-induced dissipation. $V-I$ curves show a series of discrete steps in approaching the normal state as the excitation current is gradually increased from values well below the critical current density. These observations show that single crystals of Sn cross over to quasi-1-D behavior at diameters that are ~5 times smaller than the zero-temperature coherence length.

When the same kinds of measurements were performed with Zn wires, very unusual and striking effects were observed.[44] Bulk Sn ($T_c = 3.7$ K) or In ($T_c = 3.4$ K) leads were again pressed into the top and bottom of the nanowire-filled membrane in order to penetrate any oxide layer at the tips of the wires. With Zn wires larger than 70-nm diameter, bulklike behavior was observed. That is, the bulk Sn−Zn nanowire−bulk Sn system shows two drops in series resistance upon cooling, the first at T_c of the contact metal (3.7 K) and the second at T_c of Zn (0.9 K), with zero resistance below this value. However, with nanowire diameters below 40 nm, the second, larger drop in resistance is suppressed, and the nanowire remains in the normal state down to the lowest temperature measured (0.47 K). This effect is reminiscent of the residual resistance observed below T_c with quasi-1-D Sn wires. Surprisingly, when a magnetic field is applied to drive the bulk Sn leads into the normal state, the superconductivity of the Zn nanowires returns. This behavior was quite unexpected because the ordinary proximity effect causes normal metals in contact with bulk superconductors to become superconducting at the interface. The suppression of superconductivity in the case of the nanowire system has therefore been named the "antiproximity effect."[44]

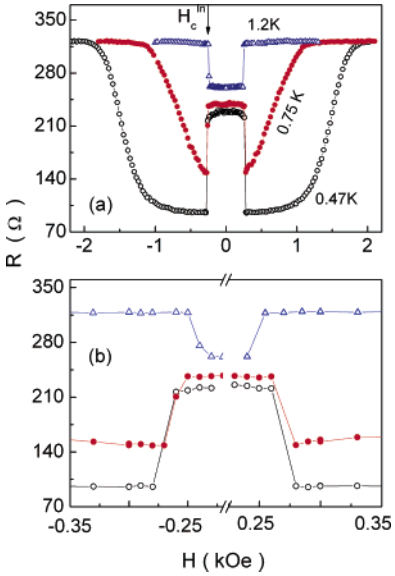

Figure 4. Resistance (R) vs field strength (H) for an individual Zn nanowire (40-nm diameter × 2-μm length) in a polycarbonate membrane, sandwiched by bulk In leads. Curves shown were obtained at 1.2, 0.75, and 0.47 K, and the figure on the right is an expanded view of the low-field region in the left figure.

Figure 4 shows $R-H$ curves illustrating the antiproximity effect for an individual Zn nanowire contacted by In leads. At 1.2 K, above T_c of Zn, there is a finite resistance at zero field, meaning that the nanowire is in the normal state. A sharp increase in resistance is seen as the field is increased beyond 0.245 ± 0.01 kOe, which corresponds to the critical field H_c for the bulk In leads. The increase in resistance reflects the change from superconducting to normal In. In the lower-temperature curves, the finite resistance at zero field shows that the Zn nanowire is normal, even though the temperature is well below its T_c (0.9 K). As the field is increased beyond H_c of the In leads, the resistance abruptly drops, signaling the normal to superconducting transition in the Zn nanowire.

(42) Giordano, N. *Phys. Rev. Lett.* **1988**, *61*, 2137; *Phys. Rev. B* **1990**, *41*, 6350; *Phys. Rev. B* **1991**, *43*, 160.
(43) Langer, J. S.; Ambegaokar, V. *Phys. Rev.* **1967**, *164*, 498. McCumber, B. E.; Halperin, B. I. *Phys. Rev. B* **1970**, *1*, 1054.
(44) Tian, M.; Kumar, N.; Xu, S.; Wang, J.; Kurtz, J. S.; Chan, M. H. W. *Phys. Rev. Lett.* **2005**, *95*, 76802.

Experiments with different contacting metals (Sn, In, Pb, and Ag) show that the antiproximity effect is quite general and can be detected whenever a quasi-1-D Zn wire is contacted at one or both ends with a bulk superconductor. Although the effect is weaker with In and Pb leads (and disappears completely for very long Zn nanowires), it can be detected in these cases as a suppression in the superconducting critical current density at low temperature. The critical current density returns to its full value when the superconducting contacts are driven to their normal state by an applied magnetic field. Work is ongoing to understand the antiproximity effect on a theoretical basis and to exploit the striking magnetoresistance behavior of superconducting nanowires in switching applications.

Optical Properties of Metal Nanowires

Metal colloids have been known since antiquity as pigments, and their optical properties have been understood at a fundamental level since the work of Mie in the early 20th century.[45] Nevertheless, metal nanoparticles are now the subject of very intensive research because of their important applications in chemical sensing, medical diagnostics and treatment, imaging, and signal processing that are enabled by their optical properties. In this context, template-grown metal nanorods offer some unique optical behavior that arises from their high aspect ratio, small size, and compositional modulation. We focus here on a few examples that illustrate these special properties.

Over the past few years, the optical properties of metal nanorods,[46−50] as well as core−shell structures,[51,52] have been extensively studied both experimentally and theoretically. The absorption spectra of Au and Ag nanoparticles contain a strong plasmon resonance, which is a collective oscillation of the delocalized electrons in the metal. The wavelength and strength of this resonance are sensitive to the size and aspect ratio of the particles, as well as to the dielectric properties of the surrounding medium. This was demonstrated by Cepak and Martin, who made high-aspect-ratio, 40−90-nm-diameter Ag and Au nanorods in polycarbonate membranes and observed the diameter dependence of the plasmon absorbance maximum.[53] Lee and El-Sayed subsequently performed detailed simulations of absorption and scattering by Au nanorods using the discrete dipole approximation method.[54] They found that the evolution of a prominent longitudinal resonance in the spectra of nanorods begins as the particles become slightly elongated, which results an increase in the imaginary part of the dielectric constant in the red and near-infrared. Experimentally, a linear relationship has been found between the absorption maximum of the longitudinal plasmon resonance and the aspect ratio of Au nanorods made by the micellar soft-template method.[55]

Some interesting consequences of strong optical absorption of metal nanorods are multipolar resonances,[56,57] nonlinear optical effects,[58] and photothermal effects[59] including optically induced reshaping.[60,61] Both the enhanced light scattering and light absorption in the red and infrared are interesting for medical imaging and therapy. Indeed, Huang, et al. have recently shown that Au nanorods, like Au nanoshells studied earlier by Halas and co-workers,[62] can act as noncytotoxic antennae for electromagnetic radiation in the tissue-transparent region of the spectrum. These particles strongly absorb near-infrared radiation, and the resulting local increase in temperature kills cancer cells in cell cultures, as well as tumors, to which they are targeted by derivatization with appropriate antibodies.[63]

As noted above, striped 1-D metal nanorods of various sequences and lengths can be fabricated in AAO templates using sequential electrochemical deposition. This additional structural control can have interesting consequences for the optical properties of the nanorods and their applications, particularly in chemical and biochemical analysis. One kind of structure with interesting optical properties is a multisegment rod containing both metal and dielectric stripes composed of self-assembled monolayers[64] or polymers.[65] When the chemical or electrochemical deposition of the organic stripe is controlled, its thickness can be adjusted between the limits of a single molecular layer (1−2 nm) or a thicker polymer layer (tens of nanometers to microns). With very thin gaps between the metal segments, the dipoles generated by longitudinal excitation interact strongly at the stripe. The strong local electric field enhancement in this geometry is of particular interest for surface-enhanced Raman spectroscopy, which has recently been studied in nanoparticle ensembles having somewhat larger (>20 nm) gaps.[66−73]

(45) Mie, G. *Ann. Phys.* **1908**, *25*, 377.
(46) Link, S.; El-Sayed, M. A. *Int. Rev. Phys. Chem.* **2000**, *19*, 409.
(47) Hao, E.; Schatz, G. C. *J. Chem. Phys.* **2004**, *120*, 357.
(48) Link, S.; El-Sayed, M. A. *Opt. Eng.* **2004**, *87*, 421.
(49) Murphy, C. J.; Sau, T. K.; Gole, A.; Orendorff, C. J. *MRS Bull.* **2005**, *30*, 349.
(50) Lee, S. J.; Morrill, A. R.; Moskovits, M. *J. Am. Chem. Soc.* **2006**, *128*, 2200.
(51) Liu, M.; Guyot-Sionnest, P. *J. Phys. Chem. B* **2004**, *108*, 5882.
(52) Ah, C. S.; Hong, S. D.; Jang, D.-J. *J. Phys. Chem. B* **2001**, *105*, 7871.
(53) Cepak, V.; Martin, C. R. *J. Phys. Chem. B* **1998**, *102*, 9985.
(54) Lee, K.-S.; El-Sayed, M. A. *J. Phys. Chem. B* **2005**, *109*, 20331.
(55) Link, S.; Mohamed, M. B.; El-Sayed, M. A. *J. Phys. Chem. B* **1999**, *103*, 3073.
(56) Laurent, G.; Felidj, N.; Aubard, J.; Levi, G.; Krenn, J. R.; Hohenau, A.; Schider, G.; Leitner, A.; Aussenegg, F. R. *J. Chem. Phys.* **2005**, *122*, 011102/1.
(57) Payne, E. K.; Shuford, K. L.; Park, S.; Schatz, G. C.; Mirkin, C. A. *J. Phys. Chem.* **2006**, ASAP article.
(58) Qu, S.; Li, H.; Peng, T.; Gao, Y.; Qiu, J.; Zhu, C. *Mater. Lett.* **2004**, *58*, 1427.
(59) Cortie, M. B.; Xu, X.; Chowdhury, H.; Zareie, H.; Smith, G. *Proc. SPIE* **2005**, *5649 (Pt. 2, Smart Structures, Devices, and Systems II)*, 565.
(60) Mohamed, M. B.; Ismail, K. Z.; Link, S.; El-Sayed, M. A. *J. Phys. Chem. B* **1998**, *102*, 9370.
(61) Chang, S.-S.; Shih, C.-W.; Chen, C.-D.; Lai, W.-C.; Wang, C. R. C. *Langmuir* **1999**, *15*, 701.
(62) (a) Halas, N. *Opt. Photonics News* **2002**, *13*, 26. (b) Hirsch, L. R.; Stafford, R. J.; Bankson, J. A.; Sershen, S. R.; Rivera, B.; Rrice, R. E.; Hazle, J. D.; Halas, N. J.; West, J. L. *Proc. Natl. Acad. Sci. U.S.A.* **2003**, *100*, 135. (c) Loo, C.; Lowery, A.; Halas, N.; West, J.; Drezek, R. *Nano Lett.* **2005**, *5*, 70.
(63) Huang, X.; El-Sayed, I. H.; Qian, W.; El-Sayed, M. A. *J. Am. Chem. Soc.* **2006**, *128*, 2115.
(64) Mbindyo, J. K. N.; Mallouk, T. E.; Mattzela, J. B.; Kratochvilova, I.; Raxavi, B.; Jackson, T. N.; Mayer, T. S. *J. Am. Chem. Soc.* **2002**, *124*, 4020.
(65) Hernandez, R. M.; Richter, L.; Semancik, S.; Stancik, S.; Mallouk, T. E. *Chem. Mater.* **2004**, *16*, 3431.

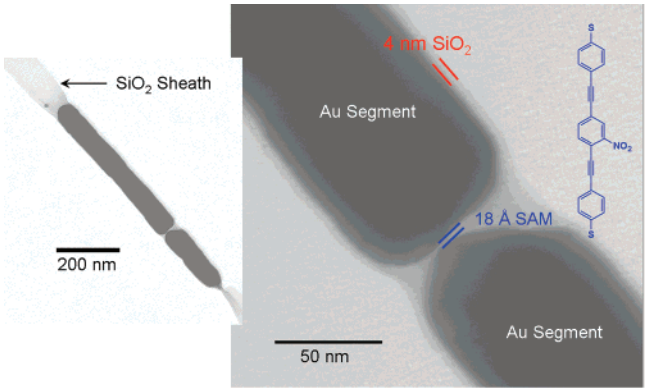

Figure 5. TEM images of a silica-encapsulated Au nanorod pair, with a gap created by adsorption of a dithiol spacer molecule between segments. The higher magnification image shows the 2-nm gap between the nanorods. Reprinted with permission from ref 75. Copyright 2005 American Physical Society.

The position and intensity of the longitudinal resonance in rod−gap−rod structures are sensitive to both the dielectric function of the material in the gap and to the shape of the opposing end caps of the rods. The end caps can be made concave, convex, or approximately flat by controlling the surface chemistry of the pore walls during electrodeposition. The growth ends of Au rods made by dc electrodeposition in AAO membranes are typically concave but can be made convex by first coating the pore with silica.[74] An example of such a structure, which contains a dithiol monolayer spacer between Au nanorods, is shown in Figure 5.[75]

Aizpurua et al. considered theoretically the interaction of light with Au rod−gap−Au rod structures as a function of several parameters (composition, length, aspect ratio, and gap length) for rods with hemispherical ends.[75] They used the boundary charge method to calculate the optical response to a plane wave with its electric vector polarized along the rod axis, in both far- and near-field approximations. Retardation (i.e., accounting for the finite speed of light) was included in the full electromagnetic calculations because some of the structures are on the order of or longer than the wavelength of light. Figure 6 shows the results of these calculations for representative gap structures. In the far field, there is strong scattering in the spectral region between 800 and 1500 nm, which corresponds to the lowest-energy dipole-active surface plasmon mode. The intensity of this band is

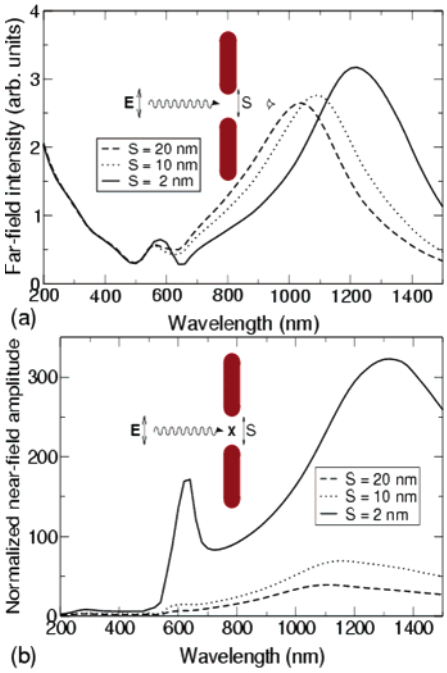

Figure 6. (a) Calculated far-field intensity for a plane wave incident on a pair of Au nanorods ($L = 200$ nm; $R = 40$ nm) with hemispherical ends separated by a gap S. (b) Calculated normalized near-field amplitude at the midpoint between the nanorods. Reprinted with permission from ref 75. Copyright 2005 American Physical Society.

relatively insensitive to the separation distance between the rod ends, but its wavelength maximum shifts to the red with decreasing separation. The shift can be understood in terms of the attractive interaction across the gap between opposite charges at the ends of the rods. This attraction damps the intrarod restoring force that drives the charge oscillation and becomes more pronounced as the size of the gap decreases. In contrast, in the near field, the scattering is strongly dependent on the size of the gap. This effect is evident in increased intensity in both the first and second dipole-active modes, in the 1200−1400- and 600-nm regions, respectively. The local electric field is dramatically increased in gaps that are on the order of the height of a self-assembled monolayer, but this effect is masked in far-field observations of scattering from the coupled nanorods. These calculations suggest that nanorod gap structures should be very interesting for field-enhanced analytical spectroscopies such as surface-enhanced Raman spectroscopy because molecules that localize in the gap (e.g., by binding to a receptor molecule that is introduced in the gap during template growth) will experience very strongly enhanced electric fields.

With multisegment metallic rods, both the surface chemistry and the optical properties (absorption and light scattering) vary with composition along the length of the rod. Figure 7 shows a bright-field image of three-segment Au−Pt−Au nanorods, in which the characteristic colors of the component metals are evident. Martin et al. demonstrated the orthogonal assembly of fluorescent and nonfluorescent molecules onto these striped rods by exploiting the differential reactivity of isonitriles and thiols.[76] Both types of

(66) Oldenburg, S. J.; Jackson, J. B.; Wescott, S. L.; Halas, N. J. *Appl. Phys. Lett.* **1999**, *75*, 2897.
(67) Jensen, R.; Schatz, G. C.; Van Duyne, R. P. *J. Phys. Chem. B* **1999**, *103*, 2394.
(68) Jin, R. C.; Cao, Y. W.; Mirkin, C. A.; Kelly, K. L.; Schatz, G. C.; Zheng, J. G. *Science* **2001**, *294*, 1901.
(69) Xu, H.; Aizpurua, J.; Käll, M.; Apell, P. *Phys. Rev. E* **2000**, *62*, 4318.
(70) Lamprecht, B.; Schider, G.; Lechner, R. T.; Ditlbacher, H.; Krenn, J. R.; Leitner, A.; Aussenegg, F. R. *Phys. Rev. Lett.* **2000**, *84*, 4721.
(71) Coyle, S.; Netti, M. C.; Baumberg, J. J.; Ghanem, M. A.; Birkin, P. R.; Bartlett, P. N.; Whittaker, D. M. *Phys. Rev. Lett.* **2001**, *87*, 176801.
(72) Mock, J. J.; Oldenburg, S. J.; Smith, D. R.; Schultz, D. A.; Schultz, S. *Nano Lett.* **2002**, *2*, 465.
(73) Taub, N.; Krichevski, O.; Markovich, G. *J. Phys. Chem. B* **2003**, *107*, 11579.
(74) Kovtyukhova, N. I.; Mallouk, T. E.; Mayer, T. S. *Adv. Mater.* **2003**, *15*, 780.
(75) Aizpurua, J.; Bryant, G. W.; Richter, L. J.; Garcia de Abajo, F. J.; Kelley, B. K.; Mallouk, T. *Phys. Rev. B* **2005**, *71*, 235420/1.
(76) Martin, B. R.; Dermody, D. J.; Reiss, B. D.; Fang, M.; Lyon, L. A.; Natan, M. J.; Mallouk, T. E. *Adv. Mater.* **1999**, *11*, 1021.

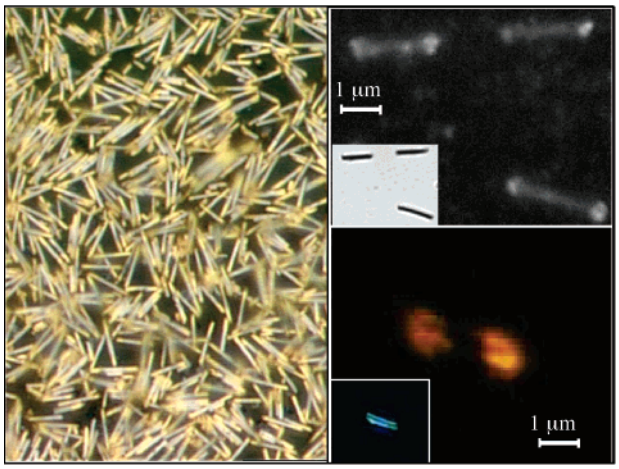

Figure 7. Optical microscope images of multisegment nanorods. Left: Bright-field image of Au−Pt−Au nanorods (from ref 76). Right: (top) Fluorescence micrograph of Au nanowires derivatized with single-strand DNA at the tips only, then removed from the alumina membrane, and hybridized with complementary fluorescent single-strand DNA; (bottom) fluorescence micrograph of striped Au−Pt−Au nanowires removed from the alumina membrane, derivatized with single-strand DNA, and then hybridized with the fluorescent complement. The insets show the corresponding bright- and dark-field images acquired in white light. Reprinted with permission from ref 78. Copyright 1999 and 2001 Wiley-VCH.

molecules adsorb to Au and to Pt surfaces, but as demonstrated in early experiments by Hickman et al.,[77] the stronger binding of thiols to Au allows one to displace the isonitrile from that surface without displacing it from Pt. Fluorescent labeling of the adsorbed thiol molecules selectively derivatized the Au ends of the rods. In subsequent experiments, it was shown that alkanethiols connected to single-strand DNA oligomers could be selectively attached to Au in multisegment nanowires and that DNA hybridization led to selective binding of rods to other rods or planar surfaces that were derivatized with complementary sequences.[78,79]

By exploiting the differential reflectivity of sequentially grown metals (e.g., Ag and Au), Keating and co-workers showed that the stripe pattern could be used as an optical barcode to identify nanorods derivatized with biomolecules in DNA and protein assays.[80−84] In this scheme, an analyte binding event is detected by conventional methods, e.g., by fluorescence microscopy. The fluorescence of a nanorod, which signals the presence of a particular analyte, is correlated with the barcode, which encodes for the receptor that is bound to that particular rod. A suspension of nanorods containing a mixture of barcodes (with their associated receptors) provides the same multiplex advantage as a microarray, in which the receptor is identified by its $x-y$ coordinates in a grid. Hence, the nanobarcode multiplexing scheme can, in principle, act as a gene chip (or protein chip) in a drop of water. Additionally, because the nanorods are not confined to a grid, they can be subjected to the kinds of manipulations that are possible with metal colloids, such as magnetic separation or dielectrophoretic binding to electrodes.[85]

Optical barcodes have distinct advantages over other optical encoding schemes, such as fluorescent tagging. They do not suffer from photobleaching, low quantum yields, broad fluorescence, and the limited number of peaks in the visible region that are associated with fluorescent organic tagging molecules. They do not require extensive modifications necessary for biocompatibility with semiconductor quantum dots[86] or the spectral limitations of color-coded microspheres.[87] With optical barcodes, the number of possible sequences is determined by the number of distinguishable stripes in the nanorod. This is subject to practical considerations of the rod length and to the Rayleigh limit of resolution $\lambda/2(\mathrm{NA})$, in which λ is the wavelength of light and NA is the numerical aperture of the microscope. Using typical values of 400 nm and 1.4 for λ and NA, respectively, this limit is 143 nm. Keating and co-workers have shown that one can obtain identification accuracies above 90%[84] with stripes down to 60 nm in length by using Ag stripes, which are 2.5 times more reflective than Au at 430 nm.[80−84] They calculate that one could encode up to 4160 analytes using stripe length variations of three metals (Ag, Au, and Pd) in a 13-segment barcode.[80]

Keating and co-workers demonstrated the utility of multisegment nanowires as nanobarcodes with sandwich DNA hybridization assays. A 24-nucleotide oligomer (the analyte) bound to a 12-nucleotide oligomer captures the sequence on the nanorods and a 12-nucleotide fluorescent probe. Fluorescence on the nanorods was not observed in the absence of the analyte oligomer.[80] They subsequently used different immunoglobulin G antibodies as capture agents and again demonstrated that selective antigen binding could be correlated with the rod barcode.[83]

One other interesting consequence of the hard-template replication method is that it can result in regular hexagonal arrays of nanorods and/or nanotubes,[88] especially if imprinting techniques are used to define the pattern in the AAO template.[16] Recently, Ag nanorod arrays of this type have been studied theoretically as optical imaging systems.[89] In these systems, the near-field components of a dipolar field can be transmitted via surface plasmon excitation through the rod array to the other side. That is, the nanowire array

(77) Hickman, J. J.; Laibinis, P. E.; Auerbach, D. I.; Zou, C.; Gardner, T. J.; Whitesides, G. M.; Wrighton, M. S. *Langmuir* **1992**, *8*, 357.
(78) Mbindyo, J. K. N.; Reiss, B. D.; Martin, B. R.; Keating, C. D.; Natan, M. J.; Mallouk, T. E. *Adv. Mater.* **2001**, *13*, 249.
(79) Reiss, B. D.; Mbindyo, J. K. N.; Martin, B. R.; Nicewarner, S. R.; Mallouk, T. E.; Natan, M. J.; Keating, C. D. *Mater. Res. Soc. Symp. Proc.* **2001**, *635*, C6.2.1.
(80) Nicewarner-Pena, S. R.; Freeman, R. G.; Reiss, B. D.; He, L.; Pena, D. J.; Walton, I. D.; Cromer, R.; Keating, C. D.; Natan, M. J. *Science* **2001**, *294*, 137.
(81) Nicewarner-Pena, S. R.; Carado, A. J.; Shale, K. E.; Keating, C. D. *J. Phys. Chem. B* **2003**, *107*, 7360.
(82) Walton, I. D.; Norton, S. M.; Balasingham, A.; He, L.; Oviso, D. F.; Gupta, D.; Raju, P. A.; Natan, M. J.; Freeman, R. G. *Anal. Chem.* **2002**, *74*, 2240.
(83) Keating, C. D.; Natan, M. J. *Adv. Mater.* **2003**, *15*, 451.
(84) Reiss, B. D.; Freeman, R. G.; Walton, I. D.; Norton, S. M.; Smith, P. C.; Stonas, W. G.; Keating, C. D.; Natan, M. J. *J. Electroanal. Chem.* **2002**, *522*, 95.
(85) Smith, P. A.; Nordquist, C. D.; Jackson, T. N.; Mayer, T. S.; Martin, B. R.; Mbindyo, J.; Mallouk, T. E. *Appl. Phys. Lett.* **2000**, *77*, 1399.
(86) Han, M.; Gao, X.; Su, J. Z.; Nie, S. *Nat. Biotechnol.* **2001**, *19*, 631.
(87) Cortese, J. D. *Scientist* **2000**, *14*, 16.
(88) Yu, S.; Li, N.; Wharton, J.; Martin, C. R. *Nano Lett.* **2003**, *3*, 81.
(89) (a) Ono, A.; Kato, J.; Kawata, S. *Phys. Rev. Lett.* **2005**, *95*, 267407/1. (b) Saj, W. M. *Proc. SPIE* **2005**, *5955 (Metamaterials)*, 143.

effectively acts as a plasmonic waveguide, transmitting an image collected in the near field with sub-wavelength resolution. The hard-template method provides a way to fabricate such arrays at the diameter and spacing needed (20−40 nm) to test these predictions.

Autonomous Movement of Metal Nanowires

One of the most challenging problems in nanotechnology is the design of power-generating engines that can drive the motion of machines on the submicron, nanoscale, and molecular levels. Synthetic organic chemistry is sufficiently sophisticated that one can now make nanoscale machines of different designs, an appealing recent example of which is a molecular car with fullerene wheels.[90] Unfortunately, such a car cannot run without an engine. Ordinary macroscopic engines, which are based on electromagnetic induction, the expansion and contraction of working fluids, etc., scale with great difficulty to these length scales. Even scalable actuators, such as piezoelectrics, conducting polymers, and environmentally responsive gels, require an external macroscopic power source and are therefore not easily integrated into small autonomously powered machines.

On the other hand, motion in biological systems, even very large ones such as ourselves, is powered entirely by molecular motors, engines with moving parts on the length scale of nanometers and below. For example, kinesin is a motor protein that actively transports intracellular cargo (mRNA, signaling molecules, etc.) along microtubules (an assembly of two proteins that acts as the track) employing adenosine triphosphate (ATP) as the "fuel".[91,92] Microtubule-based motors also power eukaryotic cell division and the flagellar motion of certain types of cells. Another class of ATP-dependent motors is based on the biopolymer actin.[93] Actin motors are responsible for the directed movement of eukaryotic cells as well as the contraction of skeletal muscle in higher organisms. *Listeria monocytogenes*, a bacterial pathogen, pushes through the cytoplasm of infected cells via the polymerization and depolymerization of actin, effectively hijacking the fuel (ATP) and the motor proteins of the host cell.[94] In all of these examples, the molecular motor locally catalyzes the metabolism of a fuel, such as ATP or GTP, and converts some of the free energy released in the reaction to mechanical energy.

One of the successful approaches to the nanoengine problem has been to adapt biological motors through appropriate genetic modification and attachment of nonbiological nanoscale parts. An early example of this hybrid approach was a bioinorganic motor employing F1-ATPase (a rotary enzyme that reversibly converts ATP to ADP) and a synthetic Ni nanorod.[95,96] This approach has the advantage of harnessing efficient and highly evolved biological engines but the disadvantage that it requires biofuels such as ATP and biofriendly buffers and temperatures.

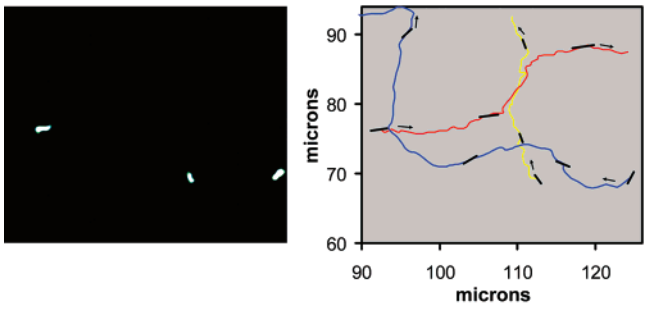

Figure 8. (B) Trajectory plots of three 2-μm-long Pt−Au rods shown in still image (A) over the following 5 s in 2.5% aqueous H_2O_2. The scale on the right is in microns. Reproduced with permission from ref 98. Copyright 2004 American Chemical Society.

An alternative approach is to consider the minimal requirements for autonomous motion and then to design fully synthetic systems that do not necessarily resemble biological motors in their form. Local catalysis of a spontaneous reaction is one essential requirement. Another is asymmetry, which is needed to generate a directional force. Ismagilov et al. first combined these features in millimeter-scale objects to demonstrate the autonomous movement of poly(dimethylsiloxane) (PDMS) objects coated at one end with Pt. The Pt catalyzed the decomposition of H_2O_2 (eq 1).[97]

$$2H_2O_2 \rightarrow 2H_2O + O_2 \qquad (1)$$

The Pt catalyst was applied as a thin film on one side of a glass "transom" of disc-shaped "boats" of PDMS, which floated on the surface of an aqueous peroxide solution. On this length scale, recoil from the generation of O_2 bubbles drove the boat at speeds of 1−2 cm/s.

Our initial experiments with nanorod motors also employed a Pt catalyst for this reaction, but as part of a striped Pt−Au nanorod approximately 350 nm in diameter and 2 μm in length. Our expectation was that the PDMS−Pt motor (powered by recoil force) would simply scale down to the micron length scale. When Pt−Au rods were added to a dilute solution of H_2O_2 (2−3.7% w/w), autonomous motion indeed occurred but the mechanism was clearly different: bubble recoil should push the rods with their Au ends forward, but axial motion in the opposite direction (Pt end forward) at speeds up to 10−20 μm/s (i.e., 5−10 body lengths/s) was observed (Figure 8).[98] Further, bubbles did not nucleate on the metal nanorods but formed instead on the surfaces of the microscope slide and coverslip that contacted the solution. Control experiments with noncatalytic Au rods and with rods lacking catalytic asymmetry (Au−Pt−Au) did not exhibit autonomous movement. Interestingly,

(90) Shirai, Y.; Osgood, A. J.; Kelley, K. F.; Tour, J. M. *Nano Lett.* **2005**, *5*, 2330.
(91) Yildiz, A.; Tomishige, M.; Vale, R. D.; Selvin, P. R. *Science* **2004**, *303*, 676.
(92) Nitta, T.; Hess, H. *Nano Lett.* **2005**, *5*, 1337.
(93) Upadhyaya, A.; Chabot, J. R.; Andreeva, A.; Samadani, A.; van Oudenaarden, A. *Proc. Natl. Acad. Sci.* **2003**, *100*, 4521.
(94) Pantaloni, D.; Le Clainche, C.; Carlier, M. *Science* **2001**, 1502.
(95) Soong, R. K.; Bachand, G. D.; Neves, H. P.; Olkhovets, A. G.; Craighead, H. G.; Montemagno, C. D. *Science* **2000**, *290*, 1555.
(96) Noji, H.; Yasuda, R.; Yoshida, M.; Kinosita, K., Jr. *Nature* **1997**, *386*, 299.
(97) Ismagilov, R. F.; Schwartz, A.; Bowden, N.; Whitesides, G. M. *Angew. Chem., Int. Ed.* **2002**, *41*, 652.
(98) Paxton, W. F.; Kistler, K. C.; Olmeda, C. C.; Sen, A.; St. Angelo, S. K.; Cao, Y.; Mallouk, T. E.; Lammert, P. E.; Crespi, V. H. *J. Am. Chem. Soc.* **2004**, *126*, 13424.

the speed and random reorientation of the motion of Pt−Au nanorods were comparable to those of multiflagellar bacteria, such as *Escherichia coli*, which are similar in size and shape.

Although it is evident that local catalysis of reaction (1) should give rise to chemical gradients (such as spatial concentration gradients of reactants and products), several mechanisms are possible for translating these gradients into forces that impel motion of nanorods. These include interfacial tension gradients, diffusiophoresis, and self-electrophoresis. At constant velocity, the force generated by catalysis must match the drag force on the cylindrical rod, which is easily calculated to be on the order of 0.01 pN.[99] Preliminary calculations showed that diffusiophoresis at the observed reaction rate [9.7(4) $\times$ 10^{-16} mol of O_2/s per rod in 2.5% H_2O_2, as measured by gas chromatography] would result in forces that are approximately 3 orders of magnitude too small. Other physical mechanisms, such as chemically generated pressure or temperature gradients, could be also eliminated because the forces they would generate would be very weak. The remaining possibilities—an interfacial tension gradient arising from the concentration gradient of O_2 along the Au segment of the rod and an electrophoretic force generated by viscous drag of protons passing through the double layer at the rod surface—were modeled and found to generate forces of the correct order of magnitude.[100] An interesting third possibility, a Brownian ratchet, has been recently suggested by Dhar et al., who studied the motion of Pt−Au nanorods confined to the air−water interface with H_2O_2 in the subphase.[101] The hypothesis in this case is that the generation of O_2 lowers the viscosity at one end of the rod. Random thermal motion of the rod can move it more easily in the direction of the less viscous fluid, and the asymmetric distribution of O_2 is reestablished after the rod moves to its new position. However, on the basis of recent tracer particle experiments conducted in an analogous catalytic micropump system,[102] the self-electrophoretic mechanism now seems most likely. In this mechanism, bipolar reduction and oxidation of H_2O_2 occur at the two ends of the rods. An asymmetry in the rates of these reactions leads to a net flow of electrons through the rod and protons through the fluid.[100] The resulting drag of water molecules by the protons results in axial rod motion, or fluid motion in the case of electrocatalyst patterns on surfaces.

The random motion of Pt−Au nanorods demonstrates the principle of autonomous motion, but these rods are not particularly useful as engines because their motion is uncontrolled. Kline et al. showed that it was possible to steer catalytically driven nanorods by incorporating ferromagnetic Ni segments in the sequential electrochemical deposition process.[103] Love et al. had shown earlier that striped metal

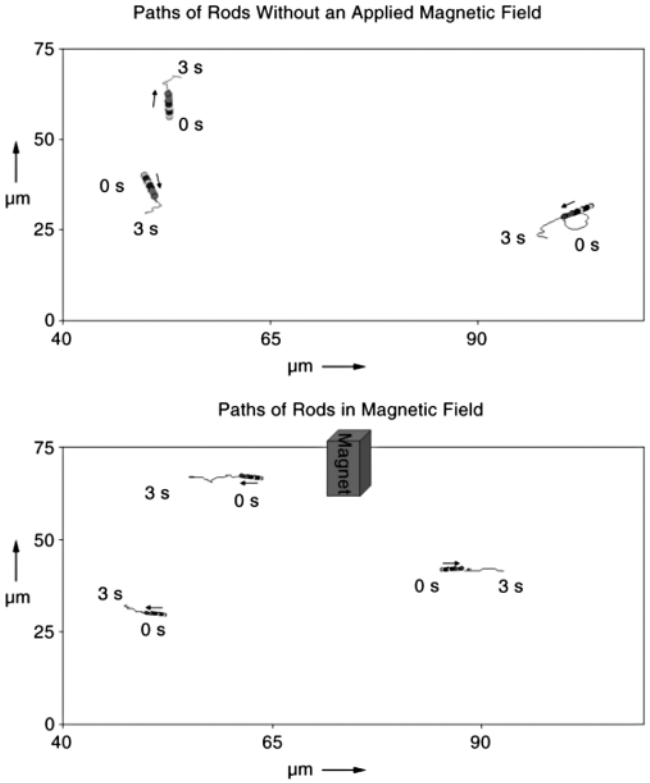

Figure 9. In-plane trajectories of rods traveling in a random fashion before applying a magnetic field (top) and the same rods traveling left or right in the presence of a field (bottom). The arrows indicate the orientation of the rods at 0 s. The field was applied by using a stack of magnets polarized in the vertical direction of the plots in the plane of the microscope stage. Reprinted with permission. Copyright 2005 Wiley-VCH.

rods containing thin ferromagnetic segments have an easy axis of magnetization perpendicular to the long axis of the rod.[104] In this configuration, an applied magnetic field orients Au−Ni−Au−Ni−Pt rods perpendicular to the field lines and does not exert a net axial force on the rod. The magnetized rods have a magnetic moment of approximately 10^{-15} A m^2, which is quite close to that of magnetotactic bacteria.[105] The influence of a small applied magnetic field on the catalyzed movement of the rods is shown in Figure 9. At a field strength of 550 G, applied by using a small stack of NdFeB magnets, the magnetic torque on the rods (7×10^{-17} N m) is about 10^4 times higher than the rotational thermal energy. Under these conditions, the rotational diffusion coefficient of the rods is drastically reduced (from 2000 to 70°^{2}/s), but their axial speed is essentially unchanged. The movement of these magnetized rods is thus confined to one direction, in much the same way as magnetotactic bacteria move in one preferred direction under the influence of the earth's magnetic field.

Several other groups have now used similar designs and synthetic strategies to achieve catalytically powered motion of nanoscale and microscale objects. Catchmark and coworkers showed that sub-millimeter scale Au gears with Pt stripes on one side of each tooth rotated at linear velocities

(99) Happel, J.; Brenner, H. *Low Reynolds Number Hydrodynamics*; Prentice Hall: Englewood Cliffs, NJ, 1965; eq 5-11.52.
(100) Paxton, W. F.; Sen, A.; Mallouk, T. E. *Chem.—Eur. J.* **2005**, *11*, 6462.
(101) Dhar, P.; Fischer, Th. M.; Wang, Y.; Mallouk, T. E.; Paxton, W. F.; Sen, A. *Nano Lett.* **2006**, *6*, 66.
(102) Kline, T. R.; Paxton, W. F.; Wang, Y.; Velegol, D.; Mallouk, T. E.; Sen, A. *J. Am. Chem. Soc.* **2005**, *127*, 17150.
(103) Kline, T. R.; Paxton, W. F.; Mallouk, T. E.; Sen, A. *Angew. Chem., Int. Ed.* **2005**, *117*, 754.
(104) Love, J. C.; Urbach, A. R.; Prentiss, M. G.; Whitesides, G. M. *J. Am. Chem. Soc.* **2003**, *125*, 12696.
(105) Lee, H.; Purdon, A. M.; Chu, V.; Westervelt, R. M. *Nano Lett.* **2004**, *4*, 995.

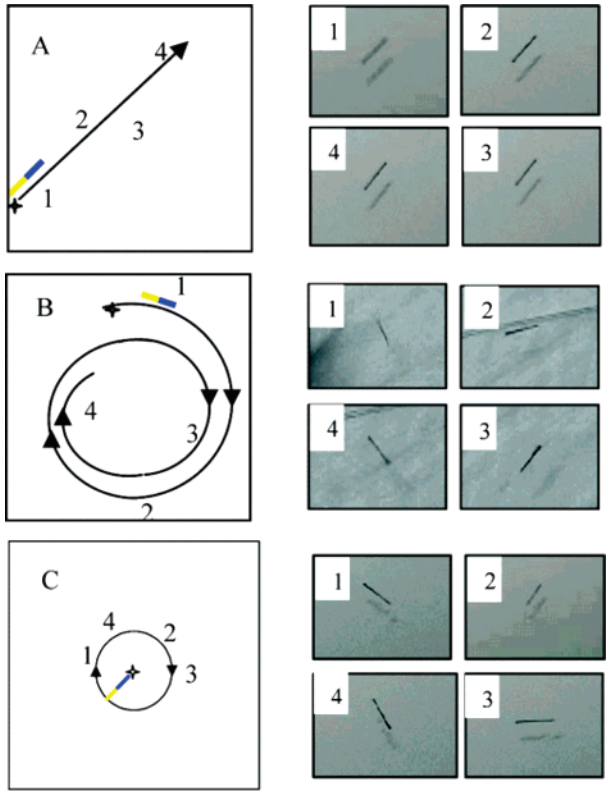

Figure 10. Graphs and images illustrating the motion of C fibers derivatized at opposite ends with glucose oxidase (GOx) and bilirubin oxidase (BOD). (A) Left: at GOx/BOD ~ 1, the trajectory is linear. Right: pictures taken at $t = 0.2$ s (1), 3 s (2), 5 s (3), and 8 s (4). (B) Left: when GOx/BOD > 1, the trajectory is spiral. Right: pictures taken at $t = 0.2$ s (1), 1 s (2), 3.8 s (3), and 6 s (4). (C) Left: when GOx/BOD $\gg$ 1, rotation around the anode is observed (blue). Right: pictures taken at $t = 1$ s (1), 7 s (2), 10 s (3), and 16 s (4). Reprinted with permission. Copyright 2005 American Chemical Society.

up to 500 μm/s in H_2O_2 solutions.[106] Fournier-Bidoz et al. observed rotational movement of Au−Ni nanorods suspended above p-type Si wafers in H_2O_2. They found that rotary motion occurred at impurities or defects on the surface of the Si, to which the Au end of the rod adhered.[107] By analogy to our experiments on the movement of tracer particles above patterned metal surfaces,[102] this movement appears to be electrokinetic in origin. That is, bipolar electrochemistry (and possibly photoelectrochemistry because the samples are illuminated by the microscope) may be occurring to generate a flux of protons between the p-type Si surface and the Ni end of the nanorods.

Recently, Mano and Heller have demonstrated the autonomous movement of C fibers derivatized at the two ends with redox enzymes (Figure 10). This was an important development in the field for two reasons. They showed, first, that a biofriendly fuel (glucose) could be used and, second, that a bipolar electrochemical reaction was unequivocally involved in energy transduction. In their system, glucose oxidase was wired to a redox-active polymer that served as the anode, oxidizing β-D-glucose to δ-glucono-1,5-lactone. Bilirubin oxidase was wired to another redox-active polymer that served as the cathode, reducing O_2 to water. The anodic reaction generates protons, which are consumed in the cathodic reaction. A conductive C fiber acts as the support for the anode and cathode, and the entire system is thus a miniaturized, short-circuited biofuel cell. In a buffered aqueous solution containing 10 mM β-D-glucose at 37 °C, the wired fibers (7 μm in diameter and 0.5−1 cm in length) moved autonomously at the air−water interface as illustrated in Figure 10. Control experiments done in the absence of O_2 (N_2 atmosphere), without glucose, or with an electronically insulating film that blocked electronic communication with the anodic enzyme resulted in no movement. Mano and Heller attributed the motion to an ion gradient that changes the surface tension at the interface, and this hypothesis was supported by altering the hydrophobicity of the wire with O_2 plasma. A hydrophilic fiber (immersed in the solution) did not move.[108]

The demonstration of an enzymatically driven rod motor is encouraging because it illustrates the possibility of using other fuels, and especially biocompatible fuels, in micro- and nanoscale engines. There is clearly much more that can be done with these systems to better understand the mechanism of their motion, to extend the idea to other types of fuels and reactions (e.g., polymerization and hydrolysis reactions, which are widely employed by biological motors), and to couple axial and rotary motors to other kinds of structures so that they can perform useful work.

Conclusions

The hard-template synthesis of metal nanorods provides an experimentally very simple route to complex and functional nanostructures. In this paper, we have covered only a few of its applications, focusing in particular on current activities in our own laboratory. Despite the fact that template synthesis has been applied over decades to a broad range of problems in nanoscale electronics, bioanalytical chemistry, magnetic materials, energy conversion, and other areas, some of the new developments in the field are quite surprising and unanticipated. This suggests that much remains to be discovered by using this method.

Acknowledgment. We thank our co-workers and collaborators, in particular Walter Paxton, Yang Wang, Paul Lammert, Shyamala Subramanian, Shakuntala Sundarajan, Nitesh Kumar, James Kurtz, Shengyong Xu, Darrell Velegol, Jeff Catchmark, Vincent Crespi, Prajna Dhar, and Thomas Fischer for their contributions to our ongoing work on catalyzed motion and superconductivity in nanowires and Brian Kelley, Javier Aizpurua, Garnett Bryant, Lee Richter, and F. J. García de Abajo for their work on the optical properties of metal nanorods. The research described herein was supported by the Penn State Center for Nanoscale Science (Grants NSF-MRSEC and DMR-021362) and was performed in part at the Penn State Nanofabrication Facility, a member of the NSF National Nanofabrication Users Network.

IC0601384

(106) Catchmark, J. M.; Subramanian, S.; Sen, A. *Small* **2005**, *1*, 202.
(107) Fournier-Bidoz, S.; Arsenault, A. C.; Manners, I.; Ozin, G. A. *Chem. Commun.* **2004**, *4*, 441.
(108) Mano, N.; Heller, A. *J. Am. Chem. Soc.* **2005**, *127*, 11574.